ELSEVIER

International Journal of Mass Spectrometry 185/186/187 (1999) 625–638

International Journal of Mass Spectrometry

The $[Re, O_8]^+$ potential energy surface: Fourier transform ion cyclotron resonance collision induced dissociation studies and density functional calculations

Martin Beyer, Christian Berg[1], Stefan Joos, Uwe Achatz, Wolfgang Hieringer[2], Gereon Niedner-Schatteburg, Vladimir E. Bondybey[3,*]

Institut für Physikalische und Theoretische Chemie, Technische Universität München, Lichtenbergstraße 4, 85747 Garching, Germany

Received 23 June 1998; accepted 29 July 1998

Abstract

As potential model systems for organometallic oxidation reaction, ions of the composition $[Re, O_n]^+$, $n = 2–6, 8$, are produced using a standard laser vaporization source and examined by Fourier transform ion cyclotron resonance collision induced dissociation mass spectrometry. Energy resolved collision induced dissociation (CID) in combination with density functional theory calculations is used to characterize the species and extract thermochemical properties. For the first time in FT-ICR, relative intensity data are converted to absolute cross sections, which are used for quantitative threshold evaluation. It is shown that $[Re, O_5]^+$ and $[Re, O_6]^+$ contain at least one, and $[Re, O_8]^+$ at least two dioxygen ligands, bound with an energy of 50–90 kJ/mol. Threshold energies in combination with the theoretical results indicate that all even-numbered species $[Re, O_{2m}]^+$ consist of O_2 ligands and can thus be written as $Re(O_2)_m^+$. $[Re, O_5]^+$ is identified as $ReO_3(O_2)^+$, the calculation yielding an end-on coordinated ligand, whereas in the $Re(O_2)_m^+$ species all ligands are side-on coordinated. (Int J Mass Spectrom 185/186/187 (1999) 625–638) © 1999 Elsevier Science B.V.

Keywords: Rhenium; O_2 ligand; Mass spectrometry; Density functional calculations; Collision induced dissociation

1. Introduction

Transition metal oxides are believed to be important intermediates in industrially relevant catalytic hydrocarbon oxidation processes, and this motivated much of the interest in their gas-phase chemistry [1]. It is, of course, necessary to note that there are considerable differences between condensed phase reactions, and processes in the collision-free environment of a mass spectrometer, and considerable caution should be exercised when transferring and applying mass spectrometric information to condensed phase catalytic processes. Nonetheless, when properly used, the mass spectrometric studies can provide useful new insights. The activation of C–H and C–C bonds by cationic transition metal monoxides has been studied in considerable detail by Fourier transform ion cyclotron resonance (FT-ICR) and

* Corresponding author.

[1] Current address: Bruker Analytical Systems, Inc., 15 Fortune Drive, Billerica, MA 01821.

[2] Current address: Institut für Anorganische Chemie, Technische Universität München.

[3] Visiting Miller Research Professor, Department of Chemistry, University of California, Berkeley, CA.

Dedicated to Professor Michael T. Bowers on the occasion of his 60th birthday.

PII S1387-3806(98)14136-2

selected ion flow tube (SIFT) mass spectrometry, and the thermochemistry involved was the subject of guided ion beam measurements [2]. Valuable insight into the behavior of more highly valent species was gained with the work of Irikura and Beauchamp on the reactivity of osmium tetroxide fragment ions [3].

In the specific case of rhenium, fragment ions of the two stable condensed phase oxides ReO_3 and Re_2O_7 have been observed in the gas phase, produced either by electron impact ionization [4] or by reactions of residual gas with the rhenium filament of mass spectrometers [5,6]. The rare earth catalyzed reaction of metallic rhenium with water was found to lead to the formation of $[Re, O_3]^-$ and $[Re_1O_4]^-$ anions in surface ionization mass spectrometry [7]. Irikura and Beauchamp observed in their study on methane activation by third row transition metal ions that ReO^+ produced in their laser ablation ion source formed $[Re, O_2]^+$ and subsequently $[Re, O_3]^+$ in binary collisions with oxygen [8].

In some oxidation processes peroxo complexes were suggested as key intermediates. For example, methylrheniumtrioxide CH_3ReO_3 catalyzed epoxidation reactions are believed to proceed via either of the two species $CH_3ReO_2(O_2)$ or $CH_3ReO(O_2)_2(H_2O)$ [9,10]. The gas phase reactivity of the $CH_3ReO_3^+$ radical cation with ethylene was investigated by Schröder et al. [11]. Cassady and McElvany have recently employed laser vaporization of solid molybdenum oxide [12] to produce the $[Mo, O_2]^+$ ion, for which they discussed a peroxo structure, but rejected it on the basis of the observed reactivity with hydrocarbons. In order to elucidate the reaction mechanism of the condensed phase epoxidation reactions and to gain further information using gas phase studies, an efficient source of ions of the type $MX(O_2)_n^{+/-}$, where M stands for the metal atom and X for additional ligands, would be desirable.

Sources combining laser vaporization [13–15] with supersonic expansion can readily be used to produce a variety of weakly bound complexes. By adding the desired ligand, e.g. N_2 or CO_2, to the carrier gas, weakly bound cationic metal compounds can be generated and spectroscopically characterized [16]. This method using molecular oxygen also turns out to be an excellent source of transition metal oxide and peroxo complex ions [17]. We have recently produced $[Re, O_n]^+$ ($n = 2–6, 8$) rhenium oxygen cations by laser vaporization and studied their ligand switching reactions with N_2 and CO_2 [18]. The present manuscript deals with the characterization of the $[Re, O_n]^+$ species by means of energy resolved collision induced dissociation (CID) [19] and by their chemical reactivity. Complementary density functional calculations are performed to provide further understanding of their structures and energetics. Throughout the text, the notation $[Re_m, O_n]^+$ is used whenever no statement about the specific structure of the ion is implied, in contrast to, e.g. ReO_2^+ or $ReO_3(O_2)^+$, which specifically denote a covalent dioxide cation and a peroxo complex of rheniumtrioxide, respectively.

Observations of the fragmentation pattern of molecular ions as a function of collision energy (CID) was shown to be a very helpful method for gaining insight into their structure and bonding [20]. Ion fragmentation was in a number of studies used to derive bond dissociation energies of a variety of compounds [21–25]. In each case, relative product intensities were used to fit the data and determine the energetic fragmentation threshold. We have recently shown that using raw intensity data may cause significant errors and that it is preferable to analyze the data using cross sections, which also depend on collision time and ion kinetic energy [19]. In the present study we apply the method to the rhenium–oxygen system in order to analyze and evaluate quantitatively the FT-ICR CID threshold data, and with the additional help of high level density functional calculations to obtain thermochemical information. One of our aims is to assess how much insight can be gained from CID about unknown species and their thermochemistry. We discuss the reliability of the data and limitations of the FT-ICR technique for energy resolved measurements.

2. Experimental and computational details

2.1. Experimental setup

The experiments were performed on a modified Spectrospin CMS47X FT-ICR mass spectrometer de-

scribed in detail elsewhere [26]. Rhenium cations ligated with oxygen of the nominal composition $[Re, O_n]^+$, n = 0–10, were produced in a disk type laser vaporization source. Only traces of the $n = 1$, 7 and >8 were present, and these species were therefore not investigated. The target material was pure rhenium, the helium carrier gas (Helium 4.6, Messer Griesheim) at 10 bar was seeded with 0.2 mbar O_2 (Sauerstoff 4.5, Messer Griesheim). The Nd:YAG laser Quanta Ray GCR3, Spectra Physics, was operated at a pulse energy of 12 mJ@532 nm with a repetition rate of 25 Hz, and focused to a 1 mm spot on the target. The metal plasma was entrained in the carrier gas pulse, cooled by flowing through a 10 mm confining channel and by subsequent supersonic expansion into high vacuum of $\sim 1 \times 10^{-4}$ mbar. The ligated rhenium cations formed were transferred through several stages of differential pumping into the high-field region of the superconducting magnet by a system of electrostatic lenses, and stored inside the ICR cell at a pressure of 6×10^{-10} mbar. Trapping voltages were 1.7 V at the first and 2.0 V at the second trapping plate. Ions of 50 injection cycles were accumulated to improve the signal to noise ratio. The argon collision gas was introduced into the ultrahigh vacuum region via a needle valve at a nominal pressure of 9.4×10^{-9} mbar, as measured at the Balzers TPG 300 ion gauge. This was converted to an absolute pressure of 3.1×10^{-8} mbar by the relative sensitivity of the ion gauge [27] and a geometry factor of 3.7 derived with the help of ion molecule reactions whose rate constants are accurately known [28]. We estimate the accuracy of the absolute pressures so determined to be about ±25%. Ion selection was achieved by applying single frequency shots, each 8 ms long with a peak-to-peak voltage of $V_{p\text{-}p}$ = 2.7 V. To avoid off-resonant excitation of the selected ions, nearby peaks, especially the second rhenium isotope, were not ejected. The selected ions were then accelerated to the desired kinetic energy by a radio frequency pulse at their resonant ICR frequency of the same fixed 2.7 V peak-to-peak voltage and variable length. Collision time in CID experiments was 1.0 s, signal acquisition took 25.6 ms.

2.2. Data evaluation

Relative rate constants of ion molecule reactions were obtained from a pseudo-first-order kinetics fit to the experimental data. These were converted to absolute rate constants and efficiencies [1] by calculating capture rates from ADO theory as described by Bowers and co-workers [29,30].

Data evaluation of CID experiments follows the procedure described in detail previously [19]. Briefly, the ion kinetic energy E_{lab} is calculated according to Comisarow and Marshall [31–34] from the ion mass m_{ed}, its charge q, and the amplitude E_1 and duration t_{exc} of the excitation pulse:

$$E_{lab} = \frac{q^2 t_{exc}^2 E_1^2}{8 m_{ed}} \tag{1}$$

For a cylindrical cell, Kofel et al. calculated the electric field amplitude E_1 from the peak to peak voltage $V_{p\text{-}p}$ of the pulse, the cell diameter d and the geometry factor S_{E1}^1 [35]:

$$E_1 = V_{p\text{-}p} S_{E1}^1 / d \tag{2}$$

E_{lab} can be converted to the center of mass energy E_{cm} of the reactant ion in collisions with a gas of mass m_{coll} by

$$E_{cm} = \frac{m_{coll}}{m_{ed} + m_{coll}} E_{lab} \tag{3}$$

Following the procedure used for data evaluation in guided ion beam (GIB) experiments in the group of Armentrout [36,37], the total cross section σ_{tot} of the collision process can be calculated from the educt intensity I_{ed} after the collisions, the sum over all product intensities I_p, the number density of the collision gas n and the length of the collision path l:

$$\sigma_{tot} = \frac{1}{nl} \ln \frac{I_{ed} + \sum I_p}{I_{ed}} \tag{4}$$

In contrast to GIB, where l is the constant length of the drift tube, l in an FT-ICR experiment depends on the ion energy, and must be computed as a product of the ion velocity with the collision time t_{coll}, and this is the crucial point in adapting the GIB approach to FT-ICR:

$$l = t_{\text{coll}} \sqrt{2 \frac{E_{\text{lab}}}{m_{\text{ed}}}} \tag{5}$$

Individual product cross sections are obtained from the total cross section σ_{tot} and the product intensities via [36]:

$$\sigma_p = \frac{I_p}{\sum I_p} \sigma_{\text{tot}} \tag{6}$$

These are fitted to the frequently used functional form of a theoretical endothermic reaction cross section that goes back to the work of Levine, Bernstein, and Rebick [38–40]:

$$\sigma(E^0_{\text{cm}}) = \sigma_0 \frac{(E^0_{\text{cm}} - E_t)^n}{E^0_{\text{cm}}} \qquad \text{for} \qquad E_{\text{cm}} \geq E_t \tag{7}$$

Here, E^0_{cm} is the kinetic energy in the center of mass of the collision partners. The fit parameters are a scaling factor σ_0, the threshold energy E_t that is to be derived, and the exponential factor n that is related to the reaction or dissociation process in question.

For better accuracy, the thermal kinetic energy distribution of the collision gas and the kinetic energy distribution of the educt ion are accounted for by convoluting $\sigma(E^0_{\text{cm}})$ with the thermal energy distribution $f(E^0_{\text{cm}}, E_{\text{cm}})$ of the collision gas according to Chantry [41] and Ervin and Armentrout [36] and the Gaussian type energy spread $P(E^{\text{ion}}_{\text{cm}}, E_{\text{cm}})$ [42] of the educt ion:

$$\sigma_{\text{eff}}(E_{\text{cm}}) = \int_0^\infty \int_{-\infty}^\infty (E^0_{\text{cm}}/E_{\text{cm}})^{1/2} P(E^{\text{ion}}_{\text{cm}}, E_{\text{cm}}) \times f(E^0_{\text{cm}}, E^{\text{ion}}_{\text{cm}}) \sigma(E^0_{\text{cm}})\, dE^{\text{ion}}_{\text{cm}}\, dE^0_{\text{cm}} \tag{8}$$

The functional form of $f(E^0_{\text{cm}}, E_{\text{cm}})$ and $P(E^{\text{ion}}_{\text{cm}}, E_{\text{cm}})$ can be found elsewhere [19]. In the present study, the ions were not extensively thermalized by e.g. pulsing in additional argon between trapping and CID excitation, and thus the assumption of an initially thermal ion kinetic energy distribution is not fully justified. However, the distribution is surely not colder than room temperature, and there are some collisions with the argon background prior to excitation. Applying the convolution thus corrects the threshold fits to a certain extent.

The fit is done by manually adjusting the three fit parameters for best agreement with the experimental data. Uncertainty limits are derived by varying σ_0 and n in order to find the highest and lowest values of threshold energies E_T which are still in acceptable agreement with the data. By this process, conservative error estimates can be achieved, i.e. the true σ_0, n and E_t values are unlikely to lie outside the so determined extremes.

These E_t values are considered to be $D_{298\ \text{K}}$ bond dissociation energies at room temperature. They are converted to D^o_0 zero Kelvin values by adding the vibrational, rotational and translational thermal energy correction of the educt ion obtained in the DFT calculations.

2.3. Computational procedure

The calculations were performed using the B3LYP [43–46] hybrid density functional method implemented in the GAUSSIAN 94 [47] program package. For geometry optimization and frequency calculation the LanL2DZ pseudo-relativistic effective core potential basis set in GAUSSIAN 94 was used on rhenium, and the D95(d) basis set on oxygen. Geometries were optimized without constraints. Stability calculations [48] were carried out on the electronic wave functions of the optimized geometry. If an instability was detected, the wavefunction was optimized, and the geometry was then reoptimized with the new wave function. The platforms used are SGI Power Challenge and DEC 400 Alpha Stations. The applicability of the B3LYP functional to transition metal complexes has been shown before [49,50].

3. Results

3.1. Typical mass spectra, stability and oxidation reactions

A typical ion distribution obtained when laser ablated rhenium is expanded in 10 bar helium with

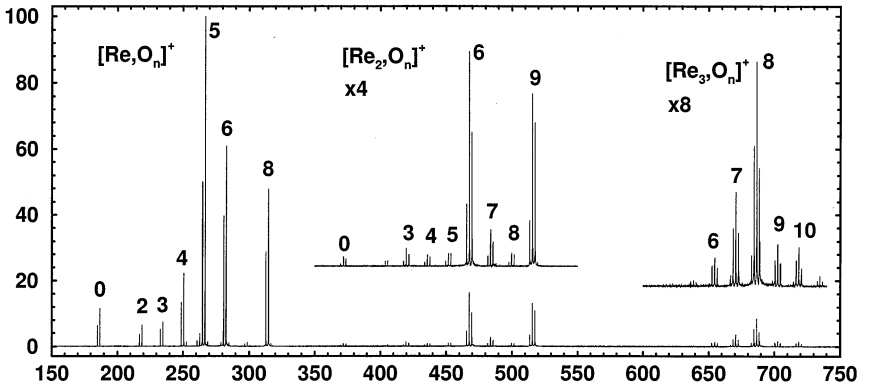

Fig. 1. Typical mass spectrum of [Re$_m$, O$_n$]$^+$ obtained by supersonic expansion of laser vaporized solid rhenium in 10 bar He seeded with O_2 at a partial pressure of 0.2 mbar. The monorhenium species contain up to eight oxygen atoms, some of them as dioxygen ligands. ReO$^+$ and [Re, O$_7$]$^+$ are at best only observed in traces. [Re$_m$, O$_n$]$^+$ ions bind up to nine oxygen atoms, with pronounced intensity maxima at $n = 6$ and $n = 9$. Again, the monoxide is missing in the spectrum. In contrast to the characteristic, irregular distributions of the mono- and dirhenium species, [Re$_3$, O$_n$]$^+$ exhibit an almost Gaussian-shaped cluster distribution, with a maximum at $n = 8$ under the conditions of this experiment.

oxygen at a partial pressure of 0.2 mbar is exemplified in Fig. 1. The distribution of cluster ions mainly depends on laser energy and O_2 concentration, and exhibits several distinct features. Most conspicuous is the consistent absence of the ReO$^+$ ion, even though [Re, O$_n$]$^+$, $n = 2$–6, 8, species are reproducibly formed in appreciable amounts. The $n = 7$ cluster is present in some spectra and absent in others, while clusters with $n > 8$ are only observable in traces. The distribution of [Re$_2$, O$_n$]$^+$ ions ends at $n = 9$, and it is lacking the [Re$_2$, O]$^+$ ion. [Re$_2$, O$_6$]$^+$ and [Re$_2$, O$_9$]$^+$ are pronounced maxima of this distribution. Species containing three rhenium atoms finally exhibit a regular cluster distribution [Re$_3$, O$_n$]$^+$, $n = 5$–11, with a maximum around $n = 8$.

To check the stability of the ions in the ICR cell against metastable decay, [Re, O$_8$]$^+$ was trapped for 60 s without collision gas or excitation. No fragmentation was observed, only reactions with the traces of water present in the cell region led to a slow formation of mainly [Re, O$_4$, H$_2$]$^+$. A second primary product of the reaction with water, [Re, O$_7$, H$_2$]$^+$ reacts very efficiently further yielding [Re, O$_5$, H$_4$]$^+$. Also when trapped in the presence of argon at a pressure of 1.9×10^{-8} mbar for 10 s, no fragmentation, and only a slow formation of the above mentioned water reaction products was detected.

In order to gain some insight into the ion formation processes, reactions of [Re, O$_n$]$^+$ with oxygen were investigated in the cell region. Only [Re, O$_2$]$^+$ was found to be reactive, forming [Re, O$_3$]$^+$ with an efficiency of 9%:

$$[\mathrm{Re, O_2}]^+ + \mathrm{O_2} \rightarrow [\mathrm{Re, O_3}]^+ + \mathrm{O} \quad (9)$$

3.2. CID results

Energy resolved CID experiments were performed for each of the [Re, O$_n$]$^+$ species, and the energy dependent cross sections calculated from reactant and fragment intensities according to Eqs. (4)–(6) are shown in Fig. 2(a)–2(f). The solid lines are cross section fits according to Eqs. (7), (8), and for [Re, O$_2$]$^+$ the "error" fits are also shown as dashed lines. The fit parameters σ_0, n and E_t are summarized in Table 1. For the neutral fragment composition it was assumed that, whenever possible, molecular oxygen is formed. Ozone formation is regarded unlikely in a collisionally excited complex in the gas phase.

The errors listed in Table 1 are solely the fitting process errors. As the ions have not been collisionally cooled prior to excitation, they may have residual kinetic energy, on which the trapping voltage places an upper limit of 1.7 eV. In the center of mass of the

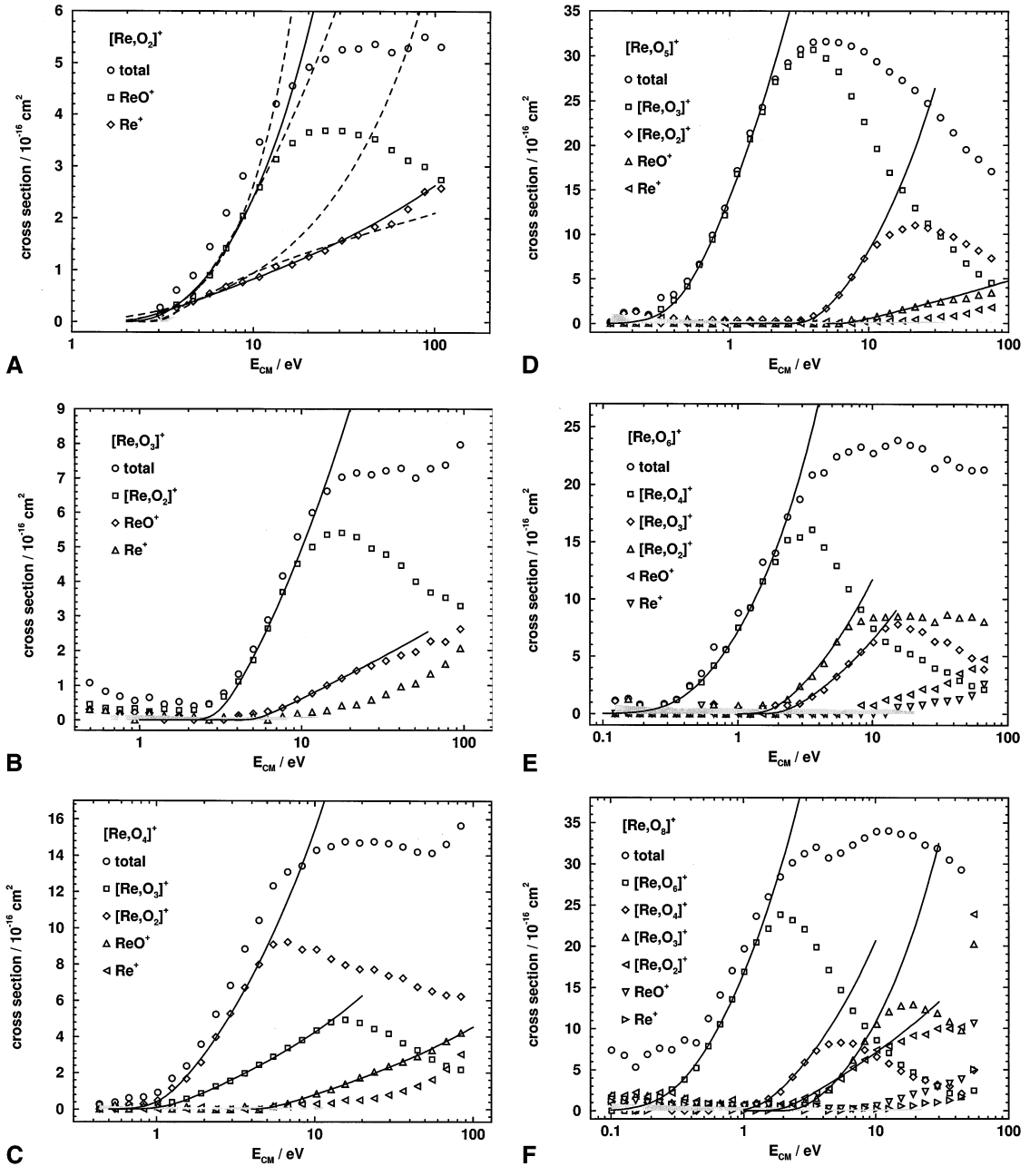

Fig. 2. Plot of absolute cross sections and threshold fits of the collision induced dissociation of (A) $[Re, O_2]^+$, (B) $[Re, O_3]^+$, (C) $[Re, O_4]^+$, (D) $[Re, O_5]^+$, (E) $[Re, O_6]^+$, and (F) $[Re, O_8]^+$. Solid lines denote fits of Eq. (8) to the experimental data. Dashed lines in (A) illustrate the error fits, which are omitted in the other figures for clarity. The absence of the $[Re, O_4]^+$ product in (D) $[Re, O_5]^+$ indicates the presence of one dioxygen ligand in $[Re, O_5]^+$, while the missing of $[Re, O_5]^+$ and $[Re, O_7]^+$ in CID of (E) $[Re, O_6]^+$ and (F) $[Re, O_8]^+$ is conclusive evidence for at least one or two O_2 ligands, respectively. The grey shaded area corresponds to the noise level.

Table 1
Fit parameters for the empirical cross section $\sigma(E) = \sigma_0(E - E_T)^n/E$, for the collision induced dissociation of $[Re, O_m]^+ \rightarrow [Re, O_n]^+ + [O_{m-n}]$, denoted (Dm,n). O_2 and O are assumed to be neutral fragments

(Dm,n)	$[Re, O_m]^+ \rightarrow [Re, O_n]^+$	σ_0	n	E_T/eV
$(D2,1)$	$[Re, O_2]^+ \rightarrow ReO^+ + O$	0.55 ± 0.80	1.85 ± 0.55	2.3 ± 0.9
$(D2,0)$	$\rightarrow Re^+ + O_2$	0.47 ± 0.48	1.38 ± 0.42	2.0 ± 1.0
$(D3,2)$	$[Re, O_3]^+ \rightarrow [Re, O_2]^+ + O$	2.5 ± 5.1	1.5 ± 0.5	2.7 ± 1.2
$(D3,1)$	$\rightarrow ReO^+ + O_2$	0.68 ± 0.72	1.35 ± 0.45	4.9 ± 1.9
$(D4,3)$	$[Re, O_4]^+ \rightarrow [Re, O_3]^+ + O$	1.75 ± 0.85	1.45 ± 0.35	1.0 ± 0.4
$(D4,2)$	$\rightarrow [Re, O_2]^+ + O_2$	5.0 ± 2.6	1.55 ± 0.35	0.9 ± 0.3
$(D4,1)$	$\rightarrow ReO^+ + O_2 + O$	0.7 ± 0.6	1.42 ± 0.58	4.5 ± 1.5
$(D5,3)$	$[Re, O_5]^+ \rightarrow [Re, O_3]^+ + O_2$	26 ± 6	1.5 ± 0.65	0.36 ± 0.16
$(D5,2)$	$\rightarrow [Re, O_2]^+ + O_2 + O$	3.5 ± 3.7	1.65 ± 0.50	3.3 ± 0.9
$(D5,1)$	$\rightarrow ReO^+ + 2O_2$	1.0 ± 1.0	1.36 ± 0.44	6.6 ± 2.1
$(D6,4)$	$[Re, O_6]^+ \rightarrow [Re, O_4]^+ + O_2$	11.5 ± 2.8	1.7 ± 0.55	0.27 ± 0.13
$(D6,3)$	$\rightarrow [Re, O_3]^+ + O_2 + O$	2.5 ± 2.2	1.55 ± 0.55	1.9 ± 0.8
$(D6,2)$	$\rightarrow [Re, O_2]^+ + 2O_2$	3.8 ± 3.9	1.6 ± 0.5	1.5 ± 0.6
$(D8,6)$	$[Re, O_8]^+ \rightarrow [Re, O_6]^+ + O_2$	24 ± 5	1.6 ± 0.6	0.23 ± 0.15
$(D8,4)$	$\rightarrow [Re, O_4]^+ + 2O_2$	6.5 ± 5.5	1.58 ± 0.72	1.1 ± 0.5
$(D8,3)$	$\rightarrow [Re, O_3]^+ + 2O_2 + O$	3.1 ± 4.9	1.73 ± 0.47	2.25 ± 0.95
$(D8,2)$	$\rightarrow [Re, O_2]^+ + 3O_2$	3.7 ± 4.1	1.4 ± 0.65	1.8 ± 1.1

argon collision gas and ions of 218–315 u, this converts to a maximum systematic error of 0.26 eV. The extracted thresholds may therefore be systematically too low by at most 25 kJ/mol.

A simple inspection of the data already reveals some interesting features. $[Re, O_2]^+$ dissociates to form both ReO^+ and Re^+ with similar threshold values of roughly 2 eV, with in fact the $[Re, O_2]^+ \rightarrow Re^+ + O_2$ channel being slightly energetically favored. This suggests that the bond in the oxygen molecule is stronger than the Re–O bond in ReO^+, making the ReO^+ formation from Re^+ and O_2 endothermic, and explaining the absence of the $n = 1$ species from the distribution formed in our source. On the other hand, the thresholds for the three fragments $[Re, O_2]^+$, ReO^+ and Re^+ observed in the fragmentation of $[Re, O_3]^+$ are quite different, with the $[Re, O_3]^+ \rightarrow [Re, O_2]^+ + O$ reaction requiring only somewhat more than 2 eV, which is about half of the energy required by the process that yields $ReO^+ + O_2$. Also $[Re, O_4]^+$ exhibits two low energy, about 1 eV, fragmentation channels. The fact that the $[Re, O_2]^+ + O_2$ threshold appears to lie somewhat below the $[Re, O_3]^+ + O$ channel is consistent with the lack of oxidation of $[Re, O_3]^+$ by molecular oxygen.

All the higher oxide ions studied, $[Re, O_5]^+$, $[Re, O_6]^+$, and $[Re, O_8]^+$ exhibit fragmentation eliminating molecular O_2, with low threshold energies around 0.5 eV and decreasing slightly with n. The alternative process, elimination of an oxygen atom, is not detected. The second fragmentation threshold of $[Re, O_8]^+$ lies near 1.1 eV, and involves elimination of two O_2 molecules.

3.3. Computational results

Optimized geometries of the oxide species ReO^+, ReO_2^+, and ReO_3^+, and of the complex oxides $ReO_3(O_2)^+$, $Re(O_2)^+$, $Re(O_2)_2^+$, $Re(O_2)_3^+$, and $Re(O_2)_4^+$ are depicted in Fig. 3. Their point groups, electronic states, B3LYP SCF energies, zero point and thermal energy corrections are summarized in Table 2. The starting geometry used for $ReO_3(O_2)^+$ was constructed by adding a side-on coordinated O_2 on top of the previously optimized ReO_3^+; this, however, distorted and tilted into the end-on structure during the geometry optimization. For $Re(O_2)_4^+$, the geometry of $Cr(O_2)_4^{3-}$ [51] was taken as starting geometry, and for $Re(O_2)_3^+$, one O_2 ligand was removed from the $Re(O_2)_4^+$ structure.

For molecules containing main group elements, B3LYP in combination with large basis sets aims at

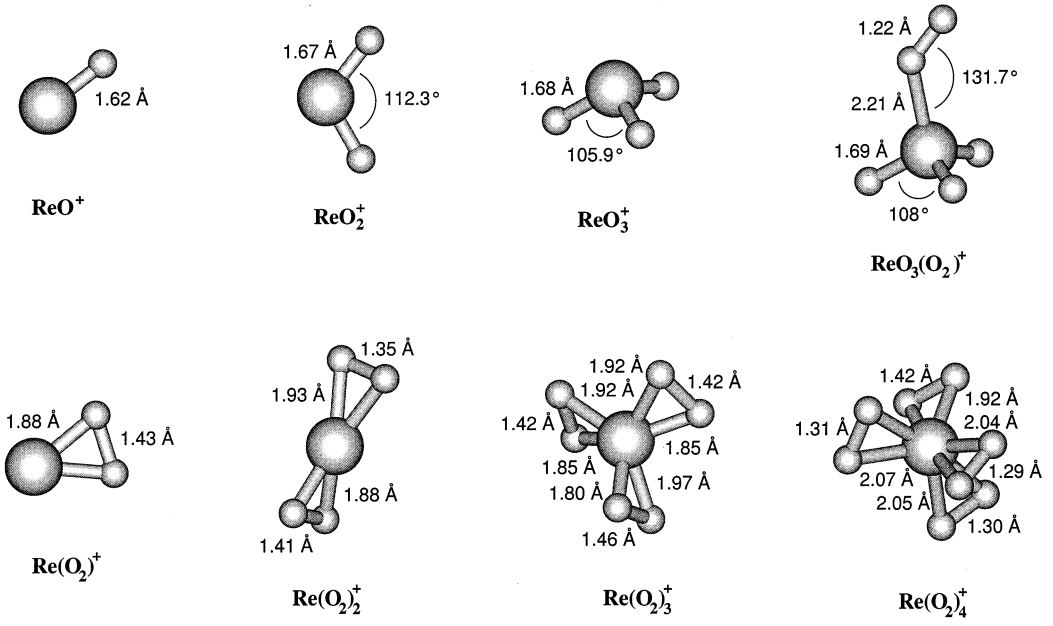

Fig. 3. Optimized geometries of various $[Re, O_n]^+$ species on the B3LYP/LanL2DZ/D95(d) level of theory. The even-numbered complex species consist of side-on coordinated O_2 ligands, while in $ReO_3(O_2)^+$, O_2 is attached end-on to ReO_3^+. Explicit coordinates are available upon request.

the so-called "chemical accuracy" of 2 kcal/mol, i.e. 10 kJ/mol. This study deals with ionic complexes of a third row transition metal, employing an only moderately large basis set without diffuse functions. Lacking thermochemical data on rhenium compounds for comparison, we expect a relative accuracy of 30% for our calculations.

3.4. Zero Kelvin bond dissociation energies, D_0^o

To derive 0 K bond dissociation energies D_0^o, the experimental E_t values are corrected by the calculated internal thermal energy from Table 2. All D_0^o values that could be derived from the E_t values are shown in Table 3. The notation (Dn,m) denotes dissociation of

Table 2
Results of the B3LYP/LanL2DZ/D95(d) calculations on $[Re, O_n]^+$. Symmetry group, electronic state, SCF energy in Hartree, zeropoint vibrational energy and thermal energy corrections in kJ/mol of the lowest energy structures shown in Fig. 3

Ion	Point group	Electronic state	SCF energy inHartree	0 K vib. energy in kJ/mol	Thermal corr. in kJ/mol
Re^+	K	$^7S_3$	−78.659 294	0	3.72
ReO^+	$C_{\infty v}$	$^3\Delta$	−153.903 903	6.95	6.25
ReO_2^+	C_{2v}	$^3B_2$	−229.194 287	14.59	8.56
$Re(O_2)^+$	C_{2v}	$^5B_1$	−229.063 204	13.30	8.33
ReO_3^+	C_{3v}	$^1A_1$	−304.457 985	25.06	10.44
$Re(O_2)_2^+$	C_{2v}	$^3A_1$	−379.505 944	29.55	14.87
$ReO_3(O_2)^+$	C_S	$^3A'$	−454.857 524	38.28	19.56
$Re(O_2)_3^+$	C_S	$^1A'$	−529.900 707	42.73	23.23
$Re(O_2)_4^+$	C_S	$^3A'$	−680.273 291	62.31	26.54
O	K	$^3P_2$	−75.083 458	0	3.72
O_2	$D_{\infty h}$	$^3\Sigma_g^-$	−150.360 612	9.86	6.21

Table 3
Bond dissociation energies in kJ/mol at 0 K obtained from Table 1 by Born-Haber cycles, corrected by the thermal energy content of the educt calculated by density functional theory. The first row shows from which experiment the values are extracted. The underlined values are considered to be the best for each dissociation process and are used in Scheme 2. In the B3LYP column, fragmentation pathways which contain $[Re, O_2]^+$ are evaluated twice. (I) denotes the ReO_2^+ dioxide structure, (II) the $Re(O_2)^+$ side-on complex

Dissociation	$[Re, O_2]^+$	$[Re, O_3]^+$	$[Re, O_4]^+$	$[Re, O_5]^+$	$[Re, O_6]^+$	$[Re, O_8]^+$	B3LYP
(*D*1,0)	483 ± 130						416.25
(*D*2,1)	**230 ± 87**	715 ± 217	347 ± 148	821 ± 222			(I) 535.77
							(II) 192.82
(*D*2,0)	**210 ± 96**						(I) 453.22
							(II) 110.27
(*D*3,2)		**271 ± 116**	494 ± 49	284 ± 88	464 ± 96	460 ± 140	(I) 462.86
(*D*3,1)		**483 ± 183**	338 ± 150	602 ± 204			499.83
(*D*4,3)			**111 ± 39**		158 ± 78	111 ± 106	−97.71
(*D*4,2)			**102 ± 29**		119 ± 59	68 ± 118	(I)−133.66
							(II) 209.29
(*D*4,1)			**449 ± 145**				402.11
(*D*5,3)				**54 ± 15**			98.87
(*D*5,2)				**338 ± 87**			(I) 561.73
(*D*5,1)				**656 ± 203**			598.70
(*D*6,4)					**49 ± 13**	84 ± 50	86.36
(*D*6,3)					**207 ± 77**	195 ± 93	−11.35
(*D*6,2)					**168 ± 58**	152 ± 107	(I) 295.65
							(II)−47.30
(*D*8,6)						**52 ± 14**	21.72
(*D*8,4)						**136 ± 48**	108.08
(*D*8,3)						**247 ± 92**	10.37
(*D*8,2)						**204 ± 106**	(I) 317.37
							(II)−25.58

$[Re, O_n]^+$ to $[Re, O_m]^+ + [O_{n-m}]$. Applying Born-Haber type cycles, one can extract dissociation energies of the individual ions from the differences in thresholds of the corresponding fragmentation processes of various larger ions. For example, the threshold of (*D*4,2), $[Re, O_4]^+ \rightarrow [Re, O_2]^+ + O_2$ can be computed as the difference of thresholds for (*D*6,2) $[Re, O_6]^+ \rightarrow [Re, O_2]^+ + 2O_2$ and (*D*6, 4) $[Re, O_6]^+ \rightarrow [Re, O_4]^+ + O_2$. In addition it was possible to derive the dissociation energy of ReO^+ (*D*1,0) in that way. The results of this calculations, converted to kJ/mol, are shown in Table 3. Numbers in bold face are the fitted values. The underlined numbers are used later to compose the potential energy surface of $[Re, O_8].^+$ For comparison, calculated B3LYP values are added, which are derived from the SCF energies corrected by the zero point vibrational energies. For processes involving $[Re, O_2]^+$, two values are given, one labelled (I) for the ReO_2^+ dioxide cation, (II) for the $Re(O_2)^+$ complex.

4. Discussion

4.1. Formation of $[Re, O_n]^+$

With the results described above, one can gain some insight into the formation of the cluster ions in the supersonic jet. Laser vaporization produces an abundance of Re^+ ions. As noted above, these ions in their ground state can for energetic reasons not form ReO^+ in thermal collisions with molecular O_2. On the other hand, direct oxidation of Re^+ to ReO_2^+ by molecular oxygen is highly exothermic, and can occur in the high pressure source with the product being collisionally stabilized. However, the complex $Re(O_2)^+$ may also be stabilized in that way, and the question is: Can we decide on the basis of our results which one of the two structures is present in the ion trap? With the help of the B3LYP results, one can calculate the 0 K reaction enthalpy of the experimentally observed oxidation reaction (9) for both cases:

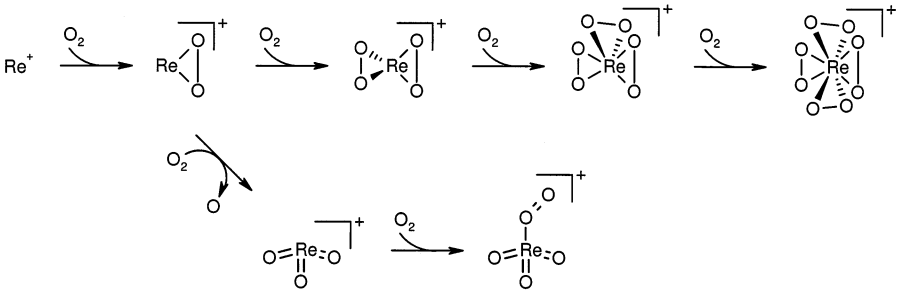

Scheme 1. Formation of $[Re,O_n]^+$ in the ion source.

$$ReO_2^+ + O_2 \rightarrow ReO_3^+ + O \qquad \Delta H_0 = +39 \text{ kJ/mol}$$
$$Re(O_2)^+ + O_2 \rightarrow ReO_3^+ + O \quad \Delta H_0 = -334 \text{ kJ/mol} \tag{10}$$

This suggests that the oxidation of the dioxide species ReO_2^+ is slightly endothermic, and one might not expect the reaction to be very efficient under the near-thermal conditions in the experiment, which does not agree with our observations. Moreover, the experimental ($D3,2$) result basically forbids the oxidation reaction (9), as the third Re–O bond yields at best only 300 kJ/mol, far less than the 500 kJ/mol required to break the O–O bond in the oxygen reactant. Furthermore, the two fragmentation pathways of $[Re, O_2]^+$, ($D2,1$), and ($D2,0$) in Table 3 exhibit energetics that are in reasonable agreement with the computed values for the $Re(O_2)^+$ complex, but far off, if the dioxide structure is assumed. These two arguments strongly favor the $Re(O_2)^+$ complex, but the presence of ReO_2^+ cannot be fully excluded. No sign for the presence of two isomers, i.e. no deviation from the pseudo-first order behavior, can be detected in the kinetics of reaction (9), where the conversion of $[Re, O_2]^+$ was followed to 80%. We have, unfortunately, not carried out isotopic exchange experiments with $^{18}O_2$, which might settle the question.

Taking the complex structure of $[Re, O_2]^+$ as a working hypothesis, the formation of the larger species is readily explained. The even-numbered $[Re, O_{2m}]^+$, $m = 1$–4, species would emerge from sequential collisional stabilization of O_2 molecules, leading to the composition $Re(O_2)_m^+$, $m = 1$–4. The clustering sequence ends with the coordinative saturation of the rhenium center at $n = 4$. ReO_3^+ is formed in reaction (9), which may proceed in the supersonic expansion of the ion source. With $Re(O_2)^+$ as a reactant, this reaction is highly exothermic, and is activated by the binding energy of the additional oxygen ligand forming a highly vibrationally excited collision complex $[Re(O_2)_2^+]$*. This can then either dissociate again, isomerize to trioxide yielding an O atom, or be collisionally stabilized, with the formation of ReO_3^+ and $Re(O_2)_2^+$ being competitive processes. This competition and the relative abundances of the two ions can be affected by parameters like laser energy or helium backing pressure, an effect we indeed observe in our experiments. The ReO_3^+ ion can bind one additional O_2 molecule, leading to the formation of $ReO_3(O_2)^+$. All the ion formation processes suggested above are summarized in Scheme 1.

Even though the experimental evidence seems to strongly favor the complex, one should be rather cautious regarding the true structure of the $[Re, O_2]^+$ species. In a recent similar study of the $[Cr, O_2]^+$ system [52], we have demonstrated clearly that the $Cr(O_2)^+$ complex may react, invisibly in the mass spectrum, with trace gases like water. The $[Cr(O_2)(H_2O)^+]$* collision complex forms transiently, with the water binding energy activating isomerization of the $Cr(O_2)^+$ complex into the thermodynamically favored CrO_2^+ chromyl cation. Thus, even though we may start with $Re(O_2)^+$ in the expansion, their interconversion into ReO_2^+ by collisions with H_2O traces cannot be fully excluded. Consequently, also some of the larger even-numbered clusters could be $ReO_2(O_2)_m^+$, instead of the

$Re(O_2)^+_{m+1}$ structure, although we consider this unlikely.

4.2. $[Re, O_8]^+$ potential energy surface

To extract the $[Re, O_8]^+$ potential energy surface from the 0 K bond dissociation energies in Table 3, it is worthwhile to examine the individual dissociation processes and discuss how reasonable the obtained values are. Thermochemical data on transition metal oxides are scarce, and especially for rhenium, no literature values are available. However, with the help of the BDEs of $D^0(Cr^+–O) = 359 \pm 12$ kJ/mol and $D^0(Mn^+–O) = 285 \pm 13$ kJ/mol derived by Fisher et al. [53], and the BDE $(W^+–O) = 524 \pm 41$ kJ/mol [54], one can crudely estimate the value for ReO^+. If the trend observed for the group 6 elements Cr and W holds also for group 7, and if the bond strengths increase from Mn to Re by a similar ratio, one could obtain BDE $(Re^+ - O) = 416 \pm 40$ kJ/mol. This is, within the error limits, in agreement with the experimental value obtained in this study, $D^o_0(Re^+–O) = 483 \pm 130$ kJ/mol, and probably in part by chance fits almost exactly with the B3LYP value of 416 kJ/mol.

The fragmentation energies of the $[Re, O_2]^+$ can be, as noted above, obtained from our data in two different ways. When derived directly from the $[Re, O_2]^+$ CID experiment, the values for $(D2,1 = 230 \pm 80$ kJ/mol) and $(D2,0 = 210 \pm 90)$ are within error limit in agreement with the B3LYP values of the complex, labeled (II) in Table 3. On the other hand, the values for $(D2,1)$ derived indirectly from the $[Re, O_3]^+$ or $[Re, O_5]^+$ experiments are much higher, and within a very large error bar in agreement with the ReO_2^+ B3LYP value of 536 kJ/mol, labeled (I) in the Table. This again supports the assumption that ReO_2^+ is formed in the fragmentation of ReO_3^+, while the $Re(O_2)^+$ complex is produced in the ion source. The $(D3,2)$ primary dissociation pathway of ReO_3^+ shows a pretty large deviation from the computed value, but agrees with the value indirectly determined from the $(D5,2)$ and $(D5,3)$ channels. If the computed ReO_2^+ energy was too low, this would account for the difference, even more so since the $(D3,1)$ values are again in agreement in theory and experiment.

The interpretation of the CID results of the larger even numbered species is a little tricky. Given the complex $Re(O_2)^+_n$ structures, it is obvious that not only ligand loss, but also chemical reactions may occur, leading to the formation of, e.g. ReO_3^+, giving rhenium its preferred +VII oxidation state. The process for which this complication does not occur is $(D4,1)$, formation of the monoxide ReO^+ from $Re(O_2)^+_2$, and the agreement with the B3LYP value is reasonably good in this case. For the other fragmentation pathways, the threshold energy may rather be seen as the activation energy needed to break the O–O bond of an O_2 ligand. Once this is accomplished, additional energy is released due to the formation of two Re–O double bonds, leading to either loss of an O_2 ligand or breaking of another O–O bond, which enables the loss of an oxygen atom. Thus it seems reasonable and consistent that the $(D4,3)$ and $(D4,2)$ pathways have almost the same threshold energy. In addition, the branching ratio favors ReO_2^+ versus ReO_3^+ in $[Re, O_4]^+$ and $[Re, O_6]^+$ fragmentations, and is only reversed in $[Re, O_8]^+$. Due to the, compared to the smaller species, larger number of degrees of freedom in $Re(O_2)^+_4$ there are more possibilities for energy redistribution, the collisionally activated complex lives longer, and the probability of the additional bond cleavage needed for ReO_3^+ formation is enhanced. The threshold energies for the loss of the first O_2 ligand from the large $[Re, O_6]^+$ and $[Re, O_8]^+$ species, $(D6,4)$ and $(D8,6)$ are lower than the activation energy discussed before, suggesting that these ligands are lost before a chemical reaction can occur.

With the low energy fragmentation pathways $(D5,3)$, $(D6,4)$, $(D8,6)$, and $(D8,4)$, which involve loss of one or two O_2 ligands, the systematic kinetic energy offset mentioned above of up to 25 kJ/mol may come into play. In addition, the B3LYP errors can be magnified as the computed energies are subtracted from each other. Taking these effects into account, we can estimate a binding energy of 50–90 kJ/mol for an additional O_2 ligand on ReO_3^+, $Re(O_2)^+_2$, and $Re(O_2)^+_3$. Both in theory and experiment, the end-on coordinated ligand in $ReO_3(O_2)^+$ is

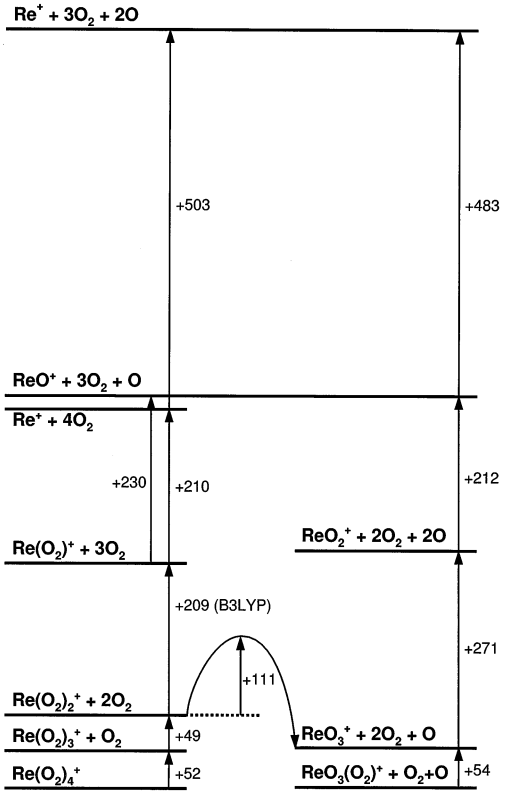

Scheme 2. $[Re,O_8]^+$ potential energy surface—CID values

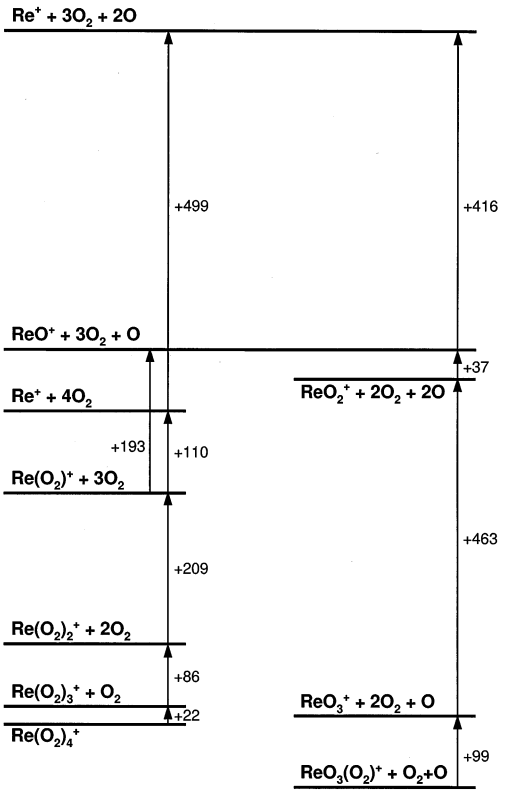

Scheme 3. $[Re,O_8]^+$ potential energy surface—B3LYP values

slightly more strongly bound than the side-on complexed O_2 in $Re(O_2)_3^+$ and $Re(O_2)_4^+$.

Selecting the most reliable experimental data, we are able to sketch the $[Re, O_8]^+$ potential energy surface as shown in Scheme 2. Due to the competing chemical reactions, we could not determine the O_2 binding energy in $Re(O_2)_2^+$, so we had to take the B3LYP value in this case. It appears somewhat high, but not unreasonably so. For comparison, the B3LYP values are used in drafting the same potential energy surface in Scheme 3. It can be seen that the two surfaces exhibit the same general features, but deviate in the absolute values.

4.3. Mode of oxygen coordination

The rather stable and abundant $[Re, O_5]^+$ cluster ion is viewed as a $ReO_3(O_2)^+$ complex, and this is confirmed by its efficient ligand exchange reactions, substituting the O_2 ligand for CO, CO_2, N_2, H_2O [18], or even methane. In comparison, $Re(O_2)_3^+$ is largely unreactive in this respect, and $Re(O_2)_4^+$ shows ligand exchange only with H_2O. This difference in behavior, as well as our B3LYP calculations support our speculation presented in the earlier communication [18] that $ReO_3(O_2)^+$ binds the oxygen ligand end-on, while the even numbered species consist of side-on coordinated O_2 ligands. In addition to the positive charge, ReO_3^+ has a pronounced dipole moment, which is certainly larger than that of $Re(O_2)_3^+$ or $Re(O_2)_2^+$. It may therefore favor an electrostatic O_2 complex against a covalent one, and this may reverse the order of relative binding energies between O_2, N_2, and CO_2, thus enabling the ligand exchange.

4.4. Advantages and limitations of energy resolved CID in FT-ICR

FT-ICR has some limitations that hamper CID experiments. In particular when an external ion source

is used, the method is not as sensitive as time of flight detection, and signal to noise ratios better than 10^3 are usually hard to achieve. When the product ion intensities are very weak, the measured relative intensities are not reliable, and processes with very low cross sections may remain completely undetected. One can increase the fragment signal by raising the collision gas pressure or extending collision time, but this can also lead to multiple collisions [55] and energy accumulation, and also enhance the effects of minor impurities. The ions are during the detection cycle accelerated to about 100 eV, and their detection takes a finite length of time. If they undergo a collision or dissociate during signal acquisition, their phase coherence will be lost, and they will not be detected.

On the other hand, there are some advantages in FT-ICR that may make it the method of choice for certain systems. Kinetic shift which may be a problem in molecular beam experiments is not as big an issue in FT-ICR [22]. While in guided ion beam experiments the time between collisional excitation and fragment detection is of the order of μs, and excited metastable ions may reach the detector before fragmenting, in FT-ICR this time is of the order of seconds and virtually all collisionally excited ions will have had time to fragment before detection. The four to five orders of magnitude lower pressure of the collision gas in the FT-ICR experiment increases the time between collisions by the same factor, and makes accumulation of energy due to multiple collisions less probable than in the guided beam experiment, as there is much more time for radiative deexcitation between the collisions.

A plot of cross sections rather than of relative intensities should be preferred even if no threshold fits are intended, since the physical quantity that carries information about the collision is the cross section, which is in principle independent of the way the experiment is done. While in a plot employing cross sections it will be obvious when this has reached a constant value, in an intensity plot such features will be obscured, since the fragment intensities will grow with increasing energy even if the cross section has reached a constant value, since the total path length covered by the ions during the constant reaction time will increase with increasing kinetic energy.

5. Conclusion

A variety of weakly bound ionic transition metal compounds and complexes can be generated in a standard laser vaporization source with supersonic expansion. We demonstrate that when properly treated, the CID cross section data from FT-ICR experiments can yield energetic thresholds and useful thermochemical information. In the present work we generate a variety of oxides of rhenium, and tentatively identify their composition as $Re(O_2)^+$, $Re(O_2)_2^+$, $Re(O_2)_3^+$, $Re(O_2)_4^+$, ReO_3^+, and $ReO_3(O_2)^+$. The structures deduced from energy resolved collisional fragmentation are in agreement with the stable structures of these species as obtained by B3LYP hybrid density functional theory calculations. The oxygen ligands are side-on coordinated in the $Re(O_2)_m^+$ species, and end-on in $ReO_3(O_2)^+$. The quality of the CID data permits us to draw a potential energy surface of the $[Re, O_8]^+$ system, which is in reasonable agreement with the energetics obtained from the DFT calculations.

Acknowledgements

Financial support from the Deutsche Forschungsgemeinschaft and the Fonds der Chemischen Industrie is gratefully acknowledged. The authors thank Wolfgang A. Herrmann for cooperation and for providing the rhenium sample.

References

[1] D. Schröder, H. Schwarz, Angew. Chemie Int. Ed. Engl. 34 (1995) 1973, and references therein.
[2] For a comparative study of the various techniques see: D. Schröder, H. Schwarz, D.E. Clemmer, Y. Chen, P.B. Armentrout, V.I. Baranov, D.K. Böhme, Int. J. Mass Spectrom. Ion Processes 161 (1997) 175.
[3] K.K. Irikura, J.L. Beauchamp, J. Am. Chem. Soc. 111 (1989) 75.

[4] H.B. Skinner, A.W. Searcy, J. Phys. Chem. 77 (1973) 1578.
[5] M.A. Grayson, Int. J. Mass. Spec. Ion Phys. 30 (1979) 383.
[6] W.J. Bouma, P.D. Burke, K.R. Jennings, Int. J. Mass Spec. Ion Phys. 36 (1980) 117.
[7] J.E. Delmore, J. Phys. Chem. 91 (1987) 2883.
[8] K.K. Irikura, J.L. Beauchamp, J. Phys. Chem. 95 (1991) 8344.
[9] W.A. Herrmann, R.W. Fischer, M.U. Rauch, W. Scherer, J. Mol. Catal. 84 (1994) 243.
[10] A.M. Al-Ajlouni, J.H. Espenson, J. Am. Chem. Soc. 177 (1995) 9243.
[11] D. Schröder, W.A. Herrmann, R.W. Fischer, H. Schwarz, Int. J. Mass Spectrom. Ion Processes 122 (1992) 99.
[12] C.J. Cassady, S.W. McElvany, Organometallics 11 (1992) 2367.
[13] V.E. Bondybey, J.H. English, J. Chem. Phys. 74 (1981) 6978.
[14] T.G. Dietz, M.A. Duncan, D.E. Powers, R.E. Smalley, J. Chem. Phys. 74 (1981) 6511.
[15] S. Maruyama, L.R. Anderson, R.E. Smalley, Rev. Sci. Instrum. 61 (1990) 3686.
[16] D.L. Robbins, L.R. Brock, J.S. Pilgrim, M.A. Duncan, J. Chem. Phys. 104 (1995) 1481.
[17] H.T. Deng, K.P. Kerns, A.W. Castleman, Jr., J. Phys. Chem. 100 (1996) 13386.
[18] M. Beyer, C. Berg, G. Albert, U. Achatz, S. Joos, G. Niedner-Schatteburg, V.E. Bondybey, J. Am. Chem. Soc. 119 (1997) 1466.
[19] M. Beyer, V.E. Bondybey, Rapid Commun. Mass Spectrom. 11 (1997) 1588.
[20] R.C. Burnier, R.B. Cody, B.S. Freiser, J. Am. Chem. Soc. 104 (1982) 7436.
[21] M. Bensimon, R. Houriet, Int. J. Mass Spectrom. Ion Processes 72 (1986) 93.
[22] A.R. Katritzky, C.H. Watson, Z. Dega-Szefran, J. Eyler, J. Am. Chem. Soc. 112 (1990) 2472.
[23] A.R. Katritzky, C.H. Watson, Z. Dega-Szefran, J. Eyler, J. Am. Chem. Soc. 112 (1990) 2479.
[24] C.E.C.A. Hop, T.B. McMahon, G.D. Willett, Int. J. Mass Spectrom. Ion Proc. 101 (1990) 191.
[25] H.L. Sievers, H.-F. Grützmacher, H. Grützmacher, S. Pitter, J. Am. Chem. Soc. 117 (1995) 2313.
[26] C. Berg, T. Schindler, G. Niedner-Schatteburg, V.E. Bondybey, J. Chem. Phys. 102 (1995) 4870.
[27] R.L. Summers, NASA Technical Note TN D-5285, National Aeronautics and Space Administration, Washington, D.C., 1969.
[28] T. Schindler, C. Berg, G. Niedner-Schatteburg, V.E. Bondybey, Ber. Bunsenges. Phys. Chem. 96 (1992) 1114.
[29] T. Su, M.T. Bowers, Int. J. Mass Spectrom. Ion Phys. 12 (1973) 347.
[30] W.J. Chesnavich, T. Su, M.T. Bowers, J. Chem. Phys. 72 (1980) 2641.
[31] M.B. Comisarow, J. Chem. Phys. 55 (1971) 205.
[32] A.G. Marshall, J. Chem. Phys. 55 (1971) 1343.
[33] M.B. Comisarow, A.G. Marshall, J. Chem. Phys. 64 (1976) 110.
[34] A.G. Marshall, D.C. Roe, J. Chem. Phys. 73 (1980) 1581.
[35] P. Kofel, M. Allemann, H.P. Kellerhals, K.-P. Wanczek, Int. J. Mass Spectrom. Ion. Processes 74 (1986) 1.
[36] K.M. Ervin, P.B. Armentrout, J. Chem. Phys. 83 (1985) 166.
[37] N. Aristov, P.B. Armentrout, J. Am. Chem. Soc. 108 (1986) 1806.
[38] R.D. Levine, R.B. Bernstein, J. Chem. Phys. 56 (1972) 281.
[39] C. Rebick, R.D. Levine, J. Chem. Phys. 58 (1973) 3492.
[40] R.D. Levine, R.B. Bernstein, Molecular Reaction Dynamics, Oxford, New York (1974), Chapt. 2.
[41] P.J. Chantry, J. Chem. Phys. 55 (1971) 2746.
[42] M. Bloom, M. Riggin, Can. J. Phys. 52 (1974) 436.
[43] A.D. Becke, Phys. Rev. A 38 (1988) 3098.
[44] A.D. Becke, J. Chem Phys. 98 (1993) 1372.
[45] A.D. Becke, J. Chem Phys. 98 (1993) 5648.
[46] P.J. Stevens, F.J. Devlin, C.F. Chablowski, M.J. Frisch, J. Phys. Chem. 98 (1994) 11623.
[47] GAUSSIAN 94, Revision D.4, M.J. Frisch, G.W. Trucks, H.B. Schlegel, P.M.W. Gill, B.G. Johnson, M.A. Robb, J.R. Cheeseman, T. Keith, G.A. Petersson, J.A. Montgomery, K. Raghavachari, M.A. Al-Laham, V.G. Zakrzewski, J.V. Ortiz, J.B. Foresman, J. Cioslowski, B.B. Stefanov, A. Nanayakkara, M. Challacombe, C.Y. Peng, P.Y. Ayala, W. Chen, M.W. Wong, J.L. Andres, E.S. Replogle, R. Gomperts, R.L. Martin, D.J. Fox, J.S. Binkley, D.J. Defrees, J. Baker, J.P. Stewart, M. Head-Gordon, C. Gonzalez, J.A. Pople, Gaussian, Inc., Pittsburgh PA, 1995.
[48] R. Bauernschmitt, R. Ahlrichs, J. Chem. Phys. 104 (1996) 9047.
[49] A. Ricca, C.W. Bauschlicher, Jr., Theor. Chim. Acta 92 (1995) 123.
[50] G. Frenking, I. Antes, M. Böhme, S. Dapprich, A.W. Ehlers, V. Jonas, A. Neuhaus, M. Otto, R. Stegmann, A. Veldkamp, S.F. Vyboishchikov, in Reviews in Computational Chemistry, Vol. 8, K.B. Lipkowitz, D.B. Boyd (Eds.), VCH, New York, 1996, p. 63.
[51] M.H. Dickman, M.T. Pope, Chem. Rev. 94 (1994) 569.
[52] M. Beyer, C. Berg, U. Achatz, S. Joos, G. Niedner-Schatteburg, V.E. Bondybey, unpublished.
[53] E.R. Fisher, J.L. Elkind, D.E. Clemmer, R. Georgiadis, S.K. Loh, N. Aristov, L.S. Sunderlin, P.B. Armentrout, J. Chem. Phys. 93 (1990) 2676.
[54] NIST Standard Reference Data Base 19A, S.G. Lias, J.F. Liebman, R.D. Levin, S.A. Kafafi, National Institute of Standards and Technology, Gaithersburg, MD 20899, Version 2.01, 1994.
[55] C.E.C.A. Hop, T.B. McMahon, G.D. Willett, Int. J. Mass Spectrom. Ion Processes 101 (1990) 191.